Journal of Physical Science Vol. 36(3), 15–25, 2025



# Investigation of the Effect of CdS Thin Films on the Optical and Structural Properties of ZnO Nanorods

Salah M. Saleh Al-Khazali<sup>1</sup> and Mohammad Malik Abood<sup>2</sup>

<sup>1</sup>The General Directorate for Education in Al-Najaf Al-Ashraf, Ministry of Education Al-Najaf, Iraq

<sup>2</sup>Department of Radiological Techniques, College of Health and Medical Technology, University of Alkafeel, Najaf, Iraq

Corresponding author: mohammadmalikmfjm@gmail.com

Published online: 28 November 2025

**To cite this article:** Saleh Al-Khazali, S. M. & Abood, M. M. (2025). Investigation of the effect of Cds thin films on the optical and structural properties of ZnO nanorods. *J. Phys. Sci.*, 36(3), 15–25. https://doi.org/10.21315/jps2025.36.3.2

To link this article: https://doi.org/10.21315/jps2025.36.3.2

**ABSTRACT:** Chemical bath deposition (CBD) was utilised to synthesise zinc oxide (ZnO) nanorods (NRs)/glass substrate arrays. On these ZnO NRs, layers of cadmium sulphide (CdS) nanoparticles (NPs) were produced using the CBD technique. The NRs in the samples grow with a highly directed (002) c-axis orientation, giving them a hexagonal tip form. CdS NPs enhance the ZnO NRs' optical absorption. According to the results, we found that the grain size decreased from 86.69 nm for ZnO to 56.62 nm after adding a layer of CdS, which may be due to the effect of the small nano-size of the CdS NPs. FE-scanning electron microscopy (SEM) examinations show that ZnO has a NR shape with an average diameter of 129 nm and a smooth surface, whereas CdS NPs/ZnO NRs have a spherical shape with an average diameter of 61 nm. The results show that the CBD method-fabricated ZnO NRs/CdS NPs provide a simple approach to nanoscale optoelectronic devices.

Keywords: CdS NPs, ZnO NRs, optical properties, heterostructures, CBD

#### 1. INTRODUCTION

The design of rational and synthesis of semiconducting nanorods (NRs) compositions and building blocks with well-defined shapes are key to making nanoelectronics and optoelectronic devices with unique features.<sup>1</sup> Due to their higher surface area and light absorption, branching heterostructures are promising nanodevice building blocks.<sup>2,3</sup> The smaller nanowire branches compared to nanowire backbones can also improve carrier separation and collecting efficiency. Zinc oxide (ZnO) nanowires on silicon (Si) substrate heterostructures have recently demonstrated high efficiency in photocathodic hydrogen production and solar water splitting.<sup>4</sup> As photoelectrochemical UV photodetectors, epitaxial titanium dioxide/tin dioxide

(TiO<sub>2</sub>/SnO<sub>2</sub>) branching heterostructures work well. As UV photodetectors, epitaxial TiO<sub>2</sub>/SnO<sub>2</sub> branching heterostructures have shown promising performance.<sup>1</sup> ZnO and cadmium sulphide (CdS) have been anticipated to be useful functional parts in photodetectors due to their good optoelectronic capabilities and direct band gaps of 3.3 and 2.4 eV, respectively. However, previous studies on CdS one-dimensional (1D) nanostructures have suffered from inadequate quantum efficiency and slow response time.<sup>5</sup> Natural imperfections, like zinc interstitials and oxygen vacancies, make UV photodetectors based on ZnO nanostructures have poor and delayed response stability of photocurrent. The photocurrent in a ZnO phase, on the other hand, is typically relatively high. 6 CdS/ZnO heterostructures have been examined to improve the photosensing efficacy of ZnO NRs. Photoelectrochemical or photocatalytic activities and solar cell applications have been reported for CdS/ZnO structures and nanocrystal-attached structures.<sup>5</sup> The produced branches on the backbones give light absorption of a higher specific surface area compared to the CdS nanoparticles (NPs), as well as photogenerated electron transport of efficient channels.<sup>7</sup> Consequently, it was interesting to investigate whether the photosensing capabilities of branching CdS/ZnO heterostructures differ from those of pure CdS backbones.8

This research, along with many others, explains why ZnO detectors are so useful and how they might be improved upon. The objective of the present work is to investigate the impact of adding a thin layer of CdS NPs on the physical characteristics of ZnO NRs and develop a simple and cost-effective method for preparing this material, which may later be used in the production of optical and gas detectors, as well as solar cells.

#### 2. METHODOLOGY

#### 2.1 Growth of ZnO NRs Array

ZnO NRs array thin film in this work was grown utilising the CBD process according to our prior study. To prepare for the deposition of the ZnO (seed layer), a 0.13 M solution was created by dissolving (Zn[CH $_3$ CO $_2$ ] $_2$ , 99% purity) in 45 mL of ethanol. The spin coating technique was employed to apply the seed solution to a glass substrate (3×3 cm²) at a speed of 3,000 rpm for 32 s, with the procedure being reproduced five times. The produced seed layer of ZnO was annealed at 250°C for 0.5 h. The samples were suspended perpendicularly inside an 85°C preheated solution consisting of 0.1 M for (Zn[NO $_3$ ] $_6$ H $_2$ O, 98% purity) and (C $_6$ H $_{12}$ N $_4$ , 99% purity) for 2.5 h in deionised water.

Once the samples had cooled to room temperature naturally, they were washed multiple times with acetone and water to remove any remaining organic residue. Annealing the produced ZnO NRs film at 300°C for 1.5 h was necessary.

# 2.2 Growth of CdS NPs on ZnO NRs Array

The CdS NPs layer was synthesised on the surface of ZnO NRs using the CBD method.

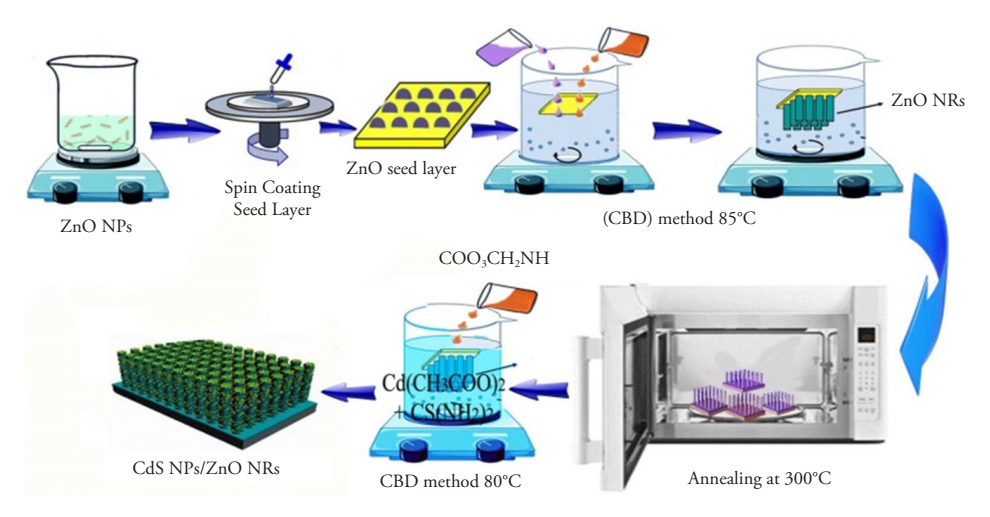


Figure 1: Diagram illustrating the process of preparing the samples.

The aqueous solution of 90 mL containing 0.05 M for bath (Cd[CH<sub>3</sub>COO]<sub>2</sub>.3H<sub>2</sub>O, 99% purity) and (CS[NH<sub>2</sub>]<sub>2</sub>, 99% purity) and 0.5 M (COO<sub>3</sub>CH<sub>2</sub>NH 98% purity) was prepared as the deposition solution. Second, the ZnO NRs array film was immersed in the deposition solution for 0.5 hours at 80°C. Finally, the samples were rinsed with ethanol multiple times before being oven dried. In this study, an X-ray diffraction (XRD) measurement was taken using an SIEMENS D500, and images of field emission scanning electron microscope (FE-SEM) were taken using an energy-dispersive X-ray spectroscopy (EDX)-equipped ZEISS SUPER 55VP. A Shimadzu-1650 UV-VIS spectrometer was used to study the optical characteristics.

#### 3. RESULTS AND DISCUSSION

# 3.1 Crystal Structure Properties

The produced samples were analysed utilising XRD to identify their crystalline structure and phase. Figure 2 presents the XRD analysis of ZnO NRs film and CdS NPs/ZnO NRs heterostructures. All of the various peaks (100), (002), (101), (102), (110), (103) and (004) for the sample synthesised in the initial stage of our work, which are represented via the pure ZnO as the (wurtzite) hexagonal phase (00-036-

1451 JCPDS). In addition to similar peaks, the CdS/ZnO film exhibits four new minor peaks that are indexed to the hexagonal planes of CdS NPs \*(100), \*(002), \*(101) and \*(110) (JCPDS 01-077-2306), demonstrating the successful creation of the CdS/ZnO heterostructure. The (002) direction is the favoured orientation for samples due to its minimal surface-free energy, which promotes nucleation. Comparable results have been documented in the literature.<sup>10</sup> The Debye-Scherrer formula was used to determine the grain size:<sup>11,12</sup>

$$D = \frac{0.9 \,\lambda}{\beta \cos \theta} \tag{1}$$

The symbol  $\lambda$  represents the wavelength, whereas the symbol  $\theta$  represents the Bragg diffraction angle and  $\beta$  is constant. The strain ( $\epsilon$ ), is directly proportional to the lattice constant (c), and its value is considered to depart from the standard value specified in the ASTM card (international standard for XRD data). This deviation may be estimated by making use of the relation that can be found in:

$$\varepsilon = \frac{|c - c_0|}{c_0} \times 100 \tag{2}$$

Where,  $(c_0)$  is the lattice constant from the XRD patterns. The value of the strain for ZnO NRs on the glass substrate was 1.351. When compared to pristine ZnO, the (002) peaks in CdS/ZnO are slightly shifted. The ZnO and CdS lattice mismatch may be to blame for this, as it causes a rise in the strain of 0.135% to 0.206% after the addition CdS layer to the ZnO film.

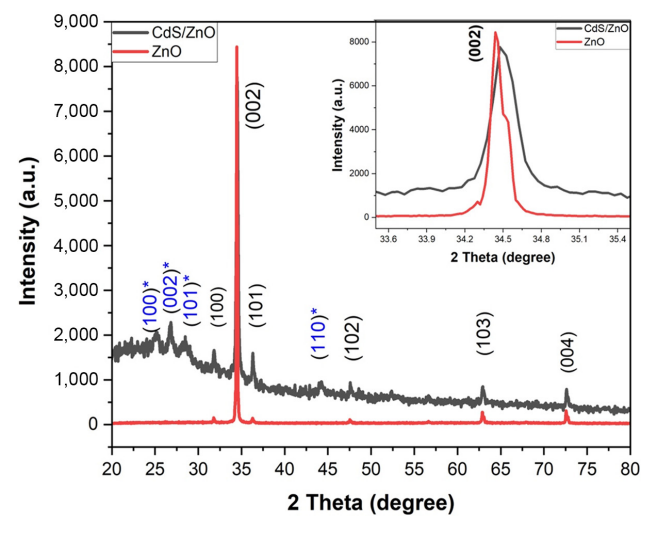


Figure 2: XRD patterns of the ZnO NRs and CdS NPs/ZnO NRs samples.

It was observed that the grain size of 86.69 nm for ZnO NR, and after adding a layer of CdS NPs, was 56.62 nm. The growth of CdS NPs on the surfaces of ZnO NRs led to the development of grainy and rough structures in the samples, in contrast to the ZnO NRs alone. This indicates that NPs were generated from the fast interactions between sulfide (S<sup>2-</sup>) anions and cadmium (Cd<sup>2+</sup>) ions during the second preparation phase.<sup>13</sup> This consequently led to the adhesion on the ZnO NR surfaces.

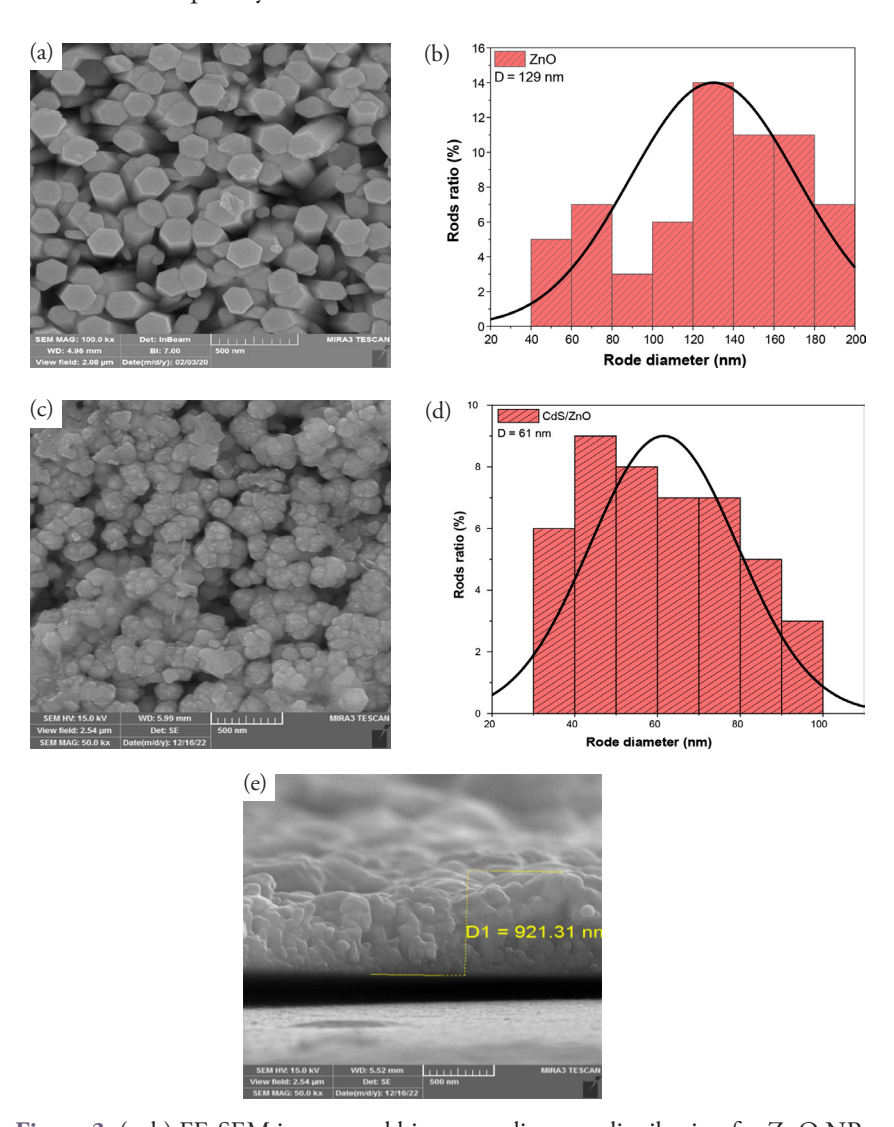


Figure 3: (a, b) FE-SEM images and histogram diameter distribution for ZnO NRs, (c, d) FE-SEM images and histogram diameter distribution for CdS NPs/ZnO NRs and (e) cross-section CdS NPs/ZnO NRs.

## 3.2 Surface Morphology

Figures 3(a–e) illustrate the FE-SEM image's top view and histogram distribution and thickness of diameters of ZnO NRs and CdS NPs/ZnO NRs films. The NR diameter of the samples was calculated using the (Image J) programme. The formed ZnO NR arrays had an average diameter of 129 nm and a smooth surface, hexagonal shape with good alignment perpendicular to the entire substrate surface.

The ZnO NRs' vertical alignment is advantageous for improving the charge transfer process in photodetector and solar cell applications. After covering with CdS NPs, spherical particles covering the entire surface of the NRs with an average diameter of 61 nm were observed in Figures 3(c–d). From the image of the cross-section in Figure 3(e), the thickness of the sample was found to be 921 nm.

Relatively recently, it has been demonstrated that defects like interphase borders and grain boundaries and doping atoms in the amorphous surficial, as well as interfacial and intergranular layers, have a significant impact on the physical characteristics of pure and doped nanostructured ZnO.<sup>14</sup> The distance between NRs affects light trapping, scattering and absorption.<sup>15</sup> Through the cross-section image, we notice that CdS covers the entire NRs, and spacing between the NRs decreases. However, for CdS/ZnO film, the length as well as the spacing between ZNRs is adequate and beneficial for photodetector performance.

The EDX spectra of ZnO NRs and CdS NPs/ZnO NRs are displayed in Figures 4 (a,b). Only carbon (C), Zn and O were discovered in the ZnO sample, accounting for 8.96%, 47.92% and 43.11% of the total weight percentages, respectively. The presence of the C element is due to the adhesive that fixes the film substrate during the EDX test. Cd, Zn, S and O components were present in the CdS/ZnO film in weight percentages of 17.83%, 53.34%, 6.67% and 23.16%, respectively. This demonstrates that a heterostructure between CdS and a ZnO nanorod was effectively produced. When comparing the two samples, the CdS/ZnO sample shows a rise and reduction in the atomic percentages of both O and Zn indicating that it would an excellent and efficient photodetector.

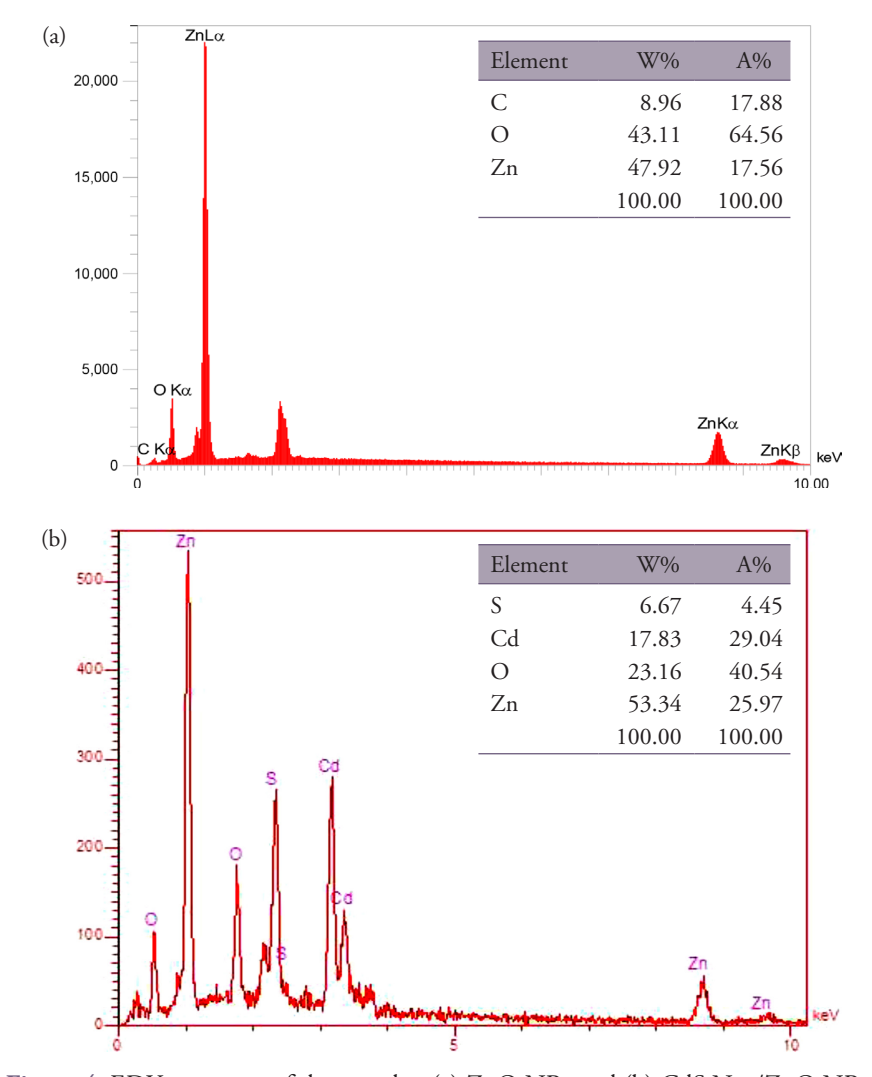
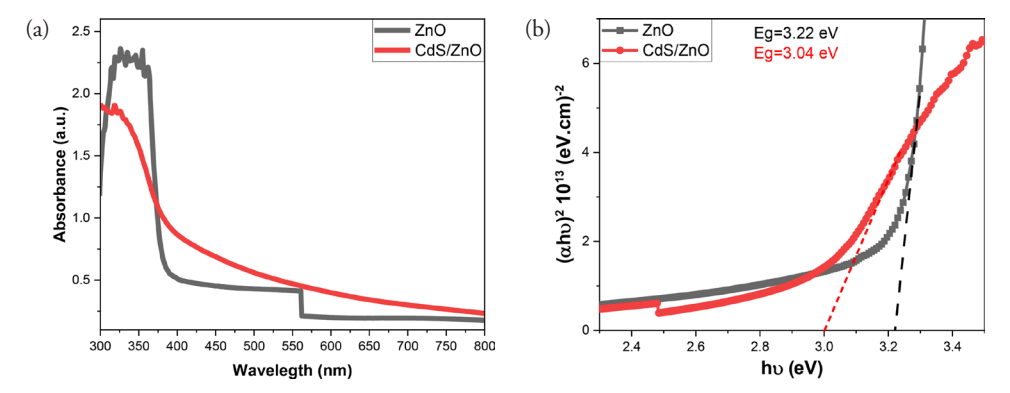


Figure 4: EDX spectrum of the samples; (a) ZnO NRs and (b) CdS Nps/ZnO NRs.

# 3.3 Optical Study

Consistent with earlier investigations, UV-Vis spectroscopy was recorded from the 300 nm to 800 nm range for both ZnO NRs and CdS NPs/ZnO NRs heterostructures (see Figure 5).<sup>10,14</sup> Figure 4(a) shows the wavelength-dependent change in optical absorbance for ZnO thin films before and after CdS NPs were deposited. ZnO NRs have an optical absorption edge of 381.5 nm. The optical absorption edge is shifted to a longer wavelength of about 407 nm (i.e., red shift) after CdS NPs have been synthesised on the surface ZnO NRs, providing further evidence of the uniformity of the fabrication NPs on the ZnO NRs' outer surface.



**Figure 5:** (a) The absorbance spectrum, and (b) plot of  $(\alpha hv)^2$  vs. hv of the ZnO NRs and CdS NPs/ZnO NRs sample.

The following equation was utilised to calculate the energy of the optical band gap: 16,17

$$\alpha h v = A_{\alpha} \left( h v - E g \right)^{1/2} \tag{3}$$

Each transition is characterised by a unique feature denoted by the symbol  $(A_{\alpha})$ , which remains unaltered by the energy of the photon. The energy of the incident photon is represented via the symbol hv. For example,  $(\alpha)$  represents the absorption coefficient, while (Eg) represents the energy bandgap.

The *Eg* of ZnO NRs was measured to be 3.22 eV (Figure 5b), which is in agreement with the value that is published in the literature. The *Eg* of CdS NPs/ZnO NRs film is shifted to 3.04 eV, as displayed in Figure 5b. The bandgap energy of CdS/ZnO film is suitable for activation via visible light. Therefore, the shift of the bandgap energy into the visible region can be attributed to the confinement effects of quantum on the semiconductor (CdS/ZnO). This finding agrees with prior research. 13,17

## 3.4 Urbach Energy

The alteration in the energy gap of bi-layer thin films can be attributed to enhanced morphology or diminished flaws. To emphasise the impact of imperfections on these films, a calculation of Urbach energy has been conducted.<sup>17</sup> The phenomenon of the absorption tail is referred to as an Urbach tail, which is directly linked to the Urbach energy. The Urbach energy is linked to localised states of amorphous structure in amorphous materials. The equation employed to compute Urbach energy is:<sup>18,19</sup>

$$\alpha = \alpha_0 \exp\left[\frac{E - E_0}{E_U}\right] \tag{4}$$

Where,  $E_U$  is the Urbach energy which quantifies the width of the band tail.  $E_0$  and  $\alpha_0$  are the coordinates at which the Urbach bundle converges. Figure 6 (a and b) demonstrates a decrease in Urbach energy from 7.63 eV to 1.54 eV when a CdS film layer is added. This decrease reflects a reduction in the structural disorder of atoms and defects. This observation is consistent with earlier studies. The decrease in Urbach energy can be attributed to enhancements in crystallisation and a minor decrease in the energy gap.

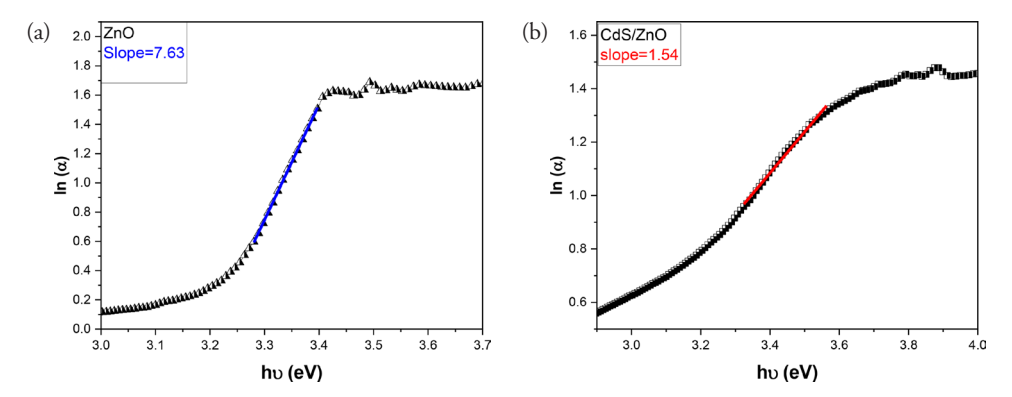


**Figure 6:** Urbach energy of (a) the ZnO NP<sub>S</sub> and (b) CdS NP<sub>S</sub>/ZnO samples.

#### 4. CONCLUSIONS

To summarise, heterostructures of CdS (NPs) and ZnO (NRs) were successfully synthesised using the CBD method. The XRD data validate the presence of a crystalline bi-layer consisting of a wurtzite structure of ZnO NRs and a hexagonal structure of CdS NPs with a grain size from 86.69 nm to 56.62 nm. The SEM analysis reveals the presence of a smooth coating with an average grain size of around 61 nm for the CdS/ZnO material. The optical bandgap of all the films was determined to be consistent with the values reported in the literature. The bandgap in the CdS/ZnO film exhibits a small reduction (3.04 eV) as compared to ZnO (3.22 eV). The Urbach energy values were computed for all of the samples, revealing that the presence of multilayer thin films can prevent disorders and charge traps. The findings indicate that the CdS/ZnO thin films exhibit superior crystallinity and shape in comparison to ZnO, with minimal alteration in the optical characteristics. The results indicate that the purpose-built (CdS NPs/ZnO NRs) heterostructures, synthesised using the CBD method, have great potential as electrode materials for optoelectronic devices.

#### 5. ACKNOWLEDGEMENTS

We extend our heartfelt appreciation to the editorial board of the Journal of Physical Science for their assistance and professionalism during the review process of our manuscript. We express our gratitude to all reviewers for their critical feedback and suggestions, which enhanced the article's quality.

The authors thank Professor Adel H. Omran Alkhayatt from the College of Medicine, University of Alkafeel, Al Najaf, Iraq, for assistance in obtaining the UV spectrophotometer for the sample.

## 6. REFERENCES

- 1. Chao, Z. et al. (2014). Photosensing performance of branched CdS/ZnO heterostructures as revealed by *in situ* TEM and photodetector tests. *Nanoscale.*, 6(14), 8084–8090. https://doi.org/10.1039/C4NR00963K
- Alireza, K. et al. (2013). Tailoring n-ZnO/p-Si branched nanowire heterostructures for selective photoelectrochemical water oxidation or reduction. *Nano Lett.*, 13(7), 3017– 3022. https://doi.org/10.1021/nl304539x
- 3. Jaafer, M. D. et al. (2020). Comparative of silver and gold nanoparticles synthesized by the chemical reduction method for antimicrobial applications. *AIP Conf. Proc.*, 2290(1), 050026. https://doi.org/10.1063/5.0027430
- 4. Ke, S. et al. (2012). 3D branched nanowire heterojunction photoelectrodes for high-efficiency solar water splitting and H<sub>2</sub> generation. *Nanoscale.*, 4(5), 1515–1521. https://doi.org/10.1039/C2NR11952H
- 5. Tianyou, Z. et al. (2009). Characterization, cathodoluminescence, and field-emission properties of morphology-tunable CdS micro/nanostructures. *Adv. Funct. Mater.*, 19(15), 2423–2430. https://doi.org/10.1002/adfm.200900295
- 6. Shize, Y. et al. (2012). The piezotronic effect of zinc oxide nanowires studied by in situ TEM. *Adv. Mater.*, 24(34), 4676–4682. https://doi.org/10.1002/adma.201104420
- 7. Kwang, H. et al. (2012). Aligned networks of cadmium sulfide nanowires for highly flexible photodetectors with improved photoconductive responses. *J. Mater. Chem.*, 22(5), 2173–2179. https://doi.org/10.1039/C2JM14359C
- 8. Wei, T. et al. (2013). Flexible SnO<sub>2</sub> hollow nanosphere film based high-performance ultraviolet photodetecto. Chem. Commun., 49(36), 3739–3741. https://doi.org/10.1039/C3CC39273B
- 9. Al-Khazali, S. M. S. et al. (2022). NO2 gas sensing performance based on ZnO nanorods synthesized by chemical bath deposition technique. *AIP Conf. Proc.*, 2398(1), 020067. https://doi.org/10.1063/5.0093783
- 10. Huey, J. T. et al. (2023). Growth-control of hexagonal CdS-decorated ZnO nanorod arrays with low-temperature preheating treatment for improved properties and efficient photoelectrochemical applications. *RSCAdv.*, 13(21), 14393–14411. https://doi.org/10.1039/D3RA01492D

- Mustafa, D. J. et al. (2019). Structural, surface topography and optical characterization of nanocrystalline Mg<sub>x</sub>Zn<sub>1-x</sub>O thin films grown by modified chemical bath deposition (SILAR) method. *J. Phys. Conf. Ser.*, 1234(1), 012001. https://doi.org/10.1088/1742 -6596/1234/1/012001
- 12. Hamid, H. A. et al. (2024). ZnO nanorods prepared by hydrothermal method as a nanosensor for methanol detection. *J. Phys. Sci.*, 35(1), 67–78. https://doi.org/10.21315/jps2024.35.1.6
- 13. Adegoke, K. A. et al. (2019). Synthesis, characterization and application of CdS/ZnO nanorod heterostructure for the photodegradation of Rhodamine B dye. *Mater. Sci. Energy Technol.*, 2(2), 329–336. https://doi.org/10.1016/j.mset.2019.02.008
- 14. Vanalakar, S. A. et al. (2014). Photoluminescence quenching of a CdS nanoparticles/ZnO nanorods core–shell heterogeneous film and its improved photovoltaic performance. *Opt. Mater.*, 37, 766–772. https://doi.org/10.1016/j.optmat.2014.09.005
- 15. Al-Khazali, S. M. S. et al. (2020). Low cost flexible ultraviolet photodetector based on ZnO nanorods prepared using chemical bath deposition. *Mater Lett.*, 277, 128177. https://doi.org/10.1016/j.matlet.2020.12817716
- Harb, N. H. et al. (2024). Preparation and characterisation of CdO@Au nanoparticles by hybrid system using laser ablation and plasma jet methods for cytotoxicity against rat embryonic fibroblast cell line. *J. Phys. Sci.*, 35(3), 17–25. https://doi.org/10.21315/ jps2024.35.3.2
- 17. Nishtha, S. et al. (2022). Equimolar ZnO-CdS nanocomposite for enhanced photocatalytic performance. *Chem. Phys. Impact*, 5, 100119. https://doi.org/10.1016/j.chphi.2022.100119
- 18. Biswajit, C. & Amarjyoti, C. (2014). Oxygen defect dependent variation of band gap, Urbach energy and luminescence property of anatase, anatase–rutile mixed phase and of rutile phases of TiO<sub>2</sub> nanoparticles. *Physica E Low Dimens. Syst. Nanostruct.*, 56, 364–371. https://doi.org/10.1016/j.physe.2013.10.014
- 19. Mohammed, R. S. et al. (2024). Synthesize of ZnO and CuO nanoparticles with plasma jet at different treatment times and testing its optical parameters with UV-Vis-NIR. *Appl. Phys.*, A. 130(533). https://doi.org/10.1007/s00339-024-07651-z
- 20. Ateyyah, M. A. et al. (2020). Structural and optical characteristic features of RF sputtered CdS/ZnO thin films. *Chinese Phys. B.*, 29(8), 080702. https://doi.org/10.1088/1674 -1056/ab90e6